Secondary Particle Showers from Hadron Absorber Interactions

Branton DeMoss
University of Colorado Boulder
High Energy Physics Group

November 14, 2015

Abstract

We simulate the contamination of muons from hadron absorber interactions in the current design of the LBNF beamline, which affects measurements relevant to accurately determining neutrino oscillation statistics. Large scale ($\sim 10^7$ Protons-On-Target) GEANT4 simulations of the current beamline geometry show that up to 10% of low energy neutrinos at the near detector come from hadron absorber interaction events. These hadron-born neutrinos are detected at the far detector much less frequently, leading to new uncertainties in the expected ratio of near to far neutrino detection events.

1 Introduction

The addition of new, complex geometry to the downstream hadron absorber in the LBNF design of the DUNE beamline could present problems related to secondary particle showers created in the absorber. Proton pulses from Fermilab's Main Injector interact with a solid graphite target to produce kaons and pions. Two focusing horns direct these products down the main decay pipe aimed at the near and far detectors. Any particles that have not decayed by the end of the pipe are stopped via interaction with the hadron absorber. This technical note discusses the secondary effects of interactions with the hadron absorber, such as secondary showers that could potentially interfere with measurement statistics. In short, we'd like to assess how secondary particles born from hadron absorber interactions affect total particle production, and whether these secondary particles contribute significant error to measurement statistics.

2 New Geometry

Recent [1] DUNE design documents have called for "scallops" to be placed in the absorber hall region. These are foot-thick aluminum blocks with spherical cuts taken out. Additionally, there is a proposal to add a foot thick solid block of aluminum to the front of the absorber region, the so-called "spoiler".

The spherical sculpts in the scallops have a radius of curvature of 0.35 meters, cut from the block such that the resultant thickness of the scallop along the beamline is 12.5 centimeters. Simulations were done with 200kA horn current and 120GeV proton energy.

Our first task was to implement the new geometry Fig. 2.1 into G4LBNE, a GEANT4 implementation of the LBNF experiment managed by Fermilab. The new geometry was implemented according mostly to [2] , with some supplementary information from Jan Boissevain's 3D model.

Most of the absorber hall region was remade to ease the implementation of the new geometry. In addition to the modifications to geometry construction source files, we created some new inputs to aid in muon and pion tracking. If our changes are added to the master branch of G4LBNE, the commands

```
/LBNE/output/doPionVertexTracking bool
/LBNE/output/doMuonVertexTracking bool
```

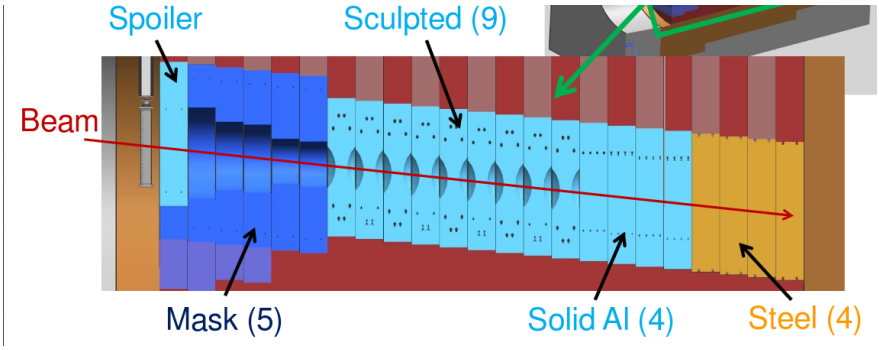

Figure 2.1: The current configuration of the absorber

will add an output Ntuple to the results file with plenty of useful information.

3 Contamination Studies

Behind the absorber hall is the "Muon alcove", inside of which are various instruments to observe stopped and through-going muons, in order to correlate muon and neutrino flux data. Therefore, if muon production rates inside the absorber volumes are not insignificant, these absorber-born muons (which are generally poor proxies for neutrinos compared to muons created in the decay pipe) will make muon/neturino correlation more difficult. Of interest, then, is the percent of all forward going muons created in absorber volumes, and their momenta distribution.

3.1 Muon Distributions

As expected, the muon profile at the tracking plane downstream of the absorber is fairly tight. If, instead of plotting the complete Fig. 3.1a distribution, we cut muons by birth position and plot only those born in absorber volumes, we find the distribution of muons born in the hadron absorber has a seemingly similar spread.

Taking the ratio of the total muon profile Fig. 3.1b to the absorber muon profile Fig. 3.1c we get a ratio plot that increases in variance with radius. This increase of variance with radius suggests that the absorber born muon distribution will be a difficult background in determining overall muon distribution statistics.

3.2 Muon counting methods

Our original method of counting muons used the detectors downstream of the absorber in the standard G4LBNE implementation. When a muon hits the detectors we get its birth position using the built-in

```
const G4ThreeVector& GetVertexPosition() const;
//See G4Track.hh for reference
```

then, we simply divide the number of muons born in absorber volumes by the total number of muons that hit the tracking plane. Using this method, we find that the muon contamination from absorber volumes is, depending on specific run settings, around 3% in the new geometry.

As a redundancy, we also used a double tracking-plane method to count muons. In this second method, we construct tracking planes both before and after the absorber hall, dividing the count of muons that hit only the back absorber by the total number that hit the back. This method gives numbers in agreement with our original method.

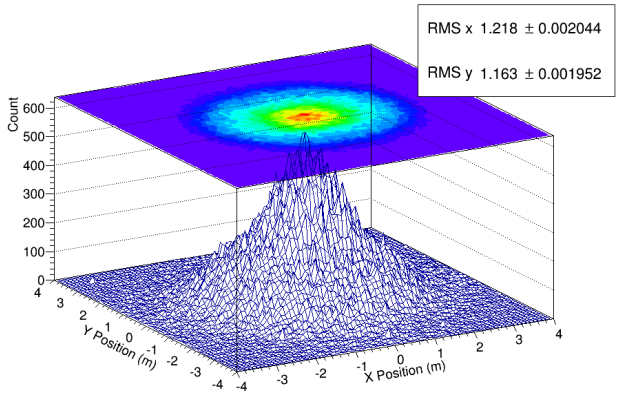

(a) Complete muon profile at tracking plane

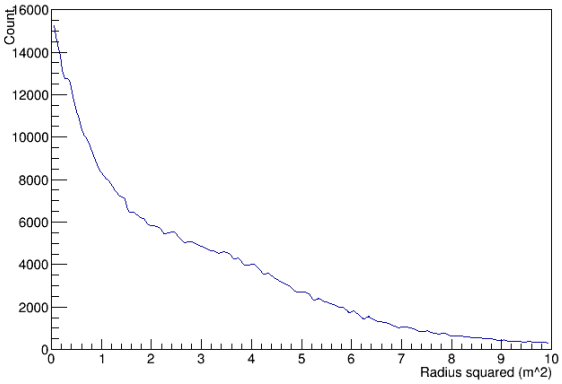

(b) Muon profile at tracking plane as a function of r^2

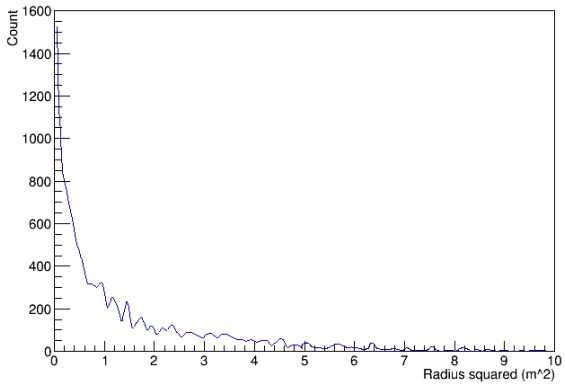

(c) Profile of absorber born muons

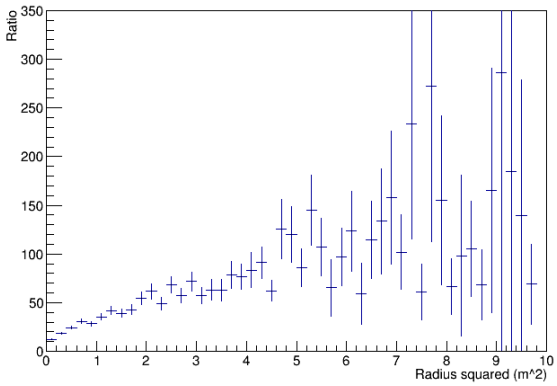

(d) Ratio of Fig. 3.1b to Fig. 3.1c

Figure 3.1: Muon profile distributions

3.3 Weighted counts

Also of interest to our studies is the degree of pion contamination from the absorber region. Here we would like to introduce a different view of what constitutes an "important" particle. Because muons are directly measured in the Muon Alcove, how their production rates change matters, neutrino production notwithstanding. Pions, however, are not directly measured, so we only consider those which are "important" with regards to how they contribute to neutrino flux at the detectors. Figure Fig. 3.2 shows pion births weighted with their eventual contribution to neutrino flux at the near detector [1], which gives us an accurate picture of how pion contamination in the absorber affects neutrino production.

There is a clear spike in "important" pion births beginning at around 220 meters, which is the start of the hadron absorber. Integrating this spike and dividing by the total pion count integral, we find that the percent of "important" pion contamination from the hadron absorber is around 0.5%.

If we weight muon births by near detector neutrino flux, we find that there is not nearly as significant a spike at the absorber hall:

Using the same pion contamination analysis as above, we find that the percent of "important" muon contamination from the absorber regions is around 0.3%.

[1] In reality we are actually counting neutrino events, weighting them with their likelihood to hit the near detector, and grabbing the parent particle birth position and type to make our "important" pion graph.

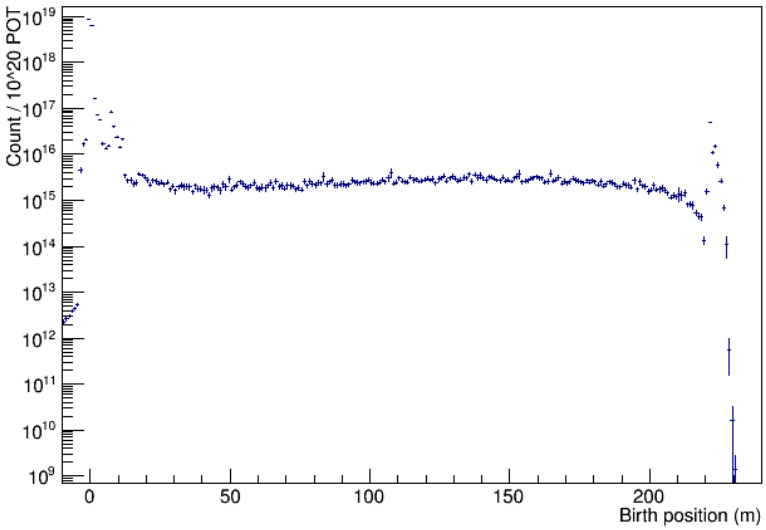

Figure 3.2: Pion births weighted with neutrino flux

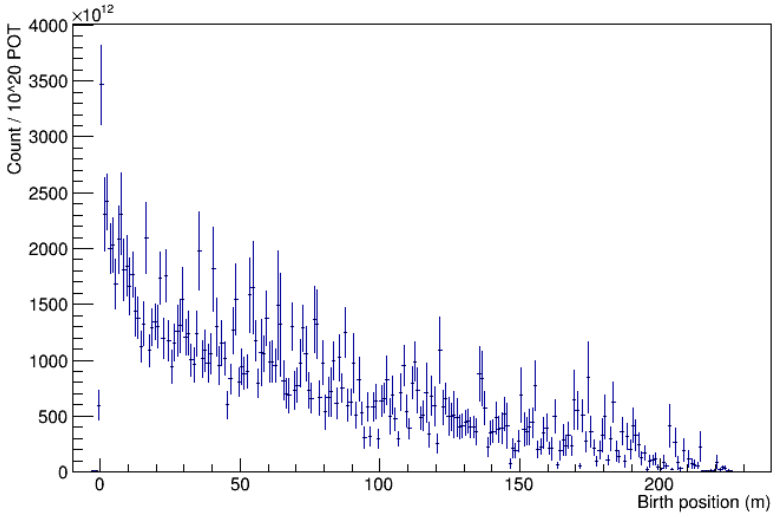

Figure 3.3: Muon births weighted with neutrino flux

Note the difference in total muon contamination (which the Muon Alcove will measure) and the "important" muon contamination.

3.4 Momentum Distributions

Both the pre-absorber Fig. 3.4 and absorber-born Fig. 3.5 muons follow a steep drop off in z-momentum at the tracking plane after passing through absorber volumes.

The momentum distribution ratio Fig. 3.6 shows that for any given momentum, the percent of muons measured at that momentum level is less than 3%, often far less.

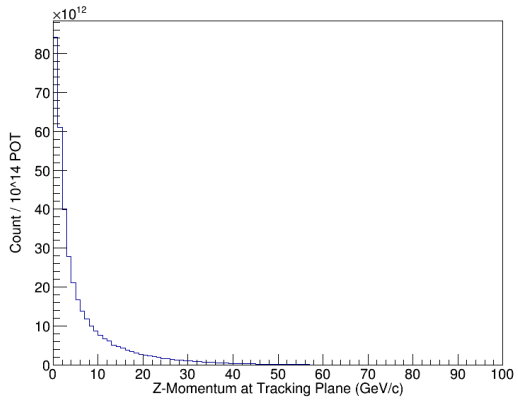

Figure 3.4: Pre-absorber muon momentum distribution

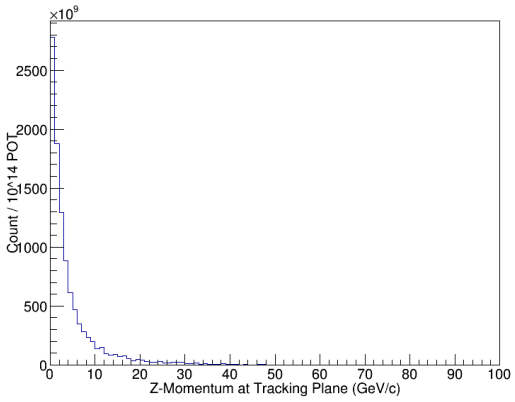

Figure 3.5: Absorber-born muon momentum distribution

Figs. 3.4 & 3.5: Momentum distributions at tracking plane

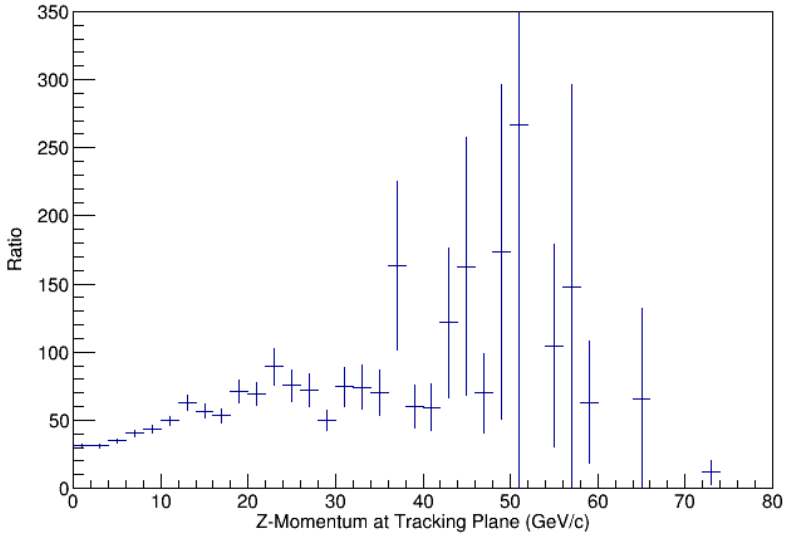

Figure 3.6: Ratio of pre-absorber to absorber muon momentum distributions

Also of interest to our study is analyzing how the hadron absorber affects muon energy distributions.

Fig. 3.7 shows how the hadron absorber tends to decrease and smooth out the energy distribution of detected muons.

4 Neutrino Flux

Of the utmost importance for this analysis is determining how neutrino flux changes with the addition of the hadron absorber. Especially, we would like to know if absorber-born neutrinos affect the near and far detection rates differently, and if so, by how much.

Our first graph Fig. 4.1 is a plot of the flux of various neutrino flavors. Comparison to similar plots [4] made for DUNE science documents shows that there are not severe differences with the new absorber

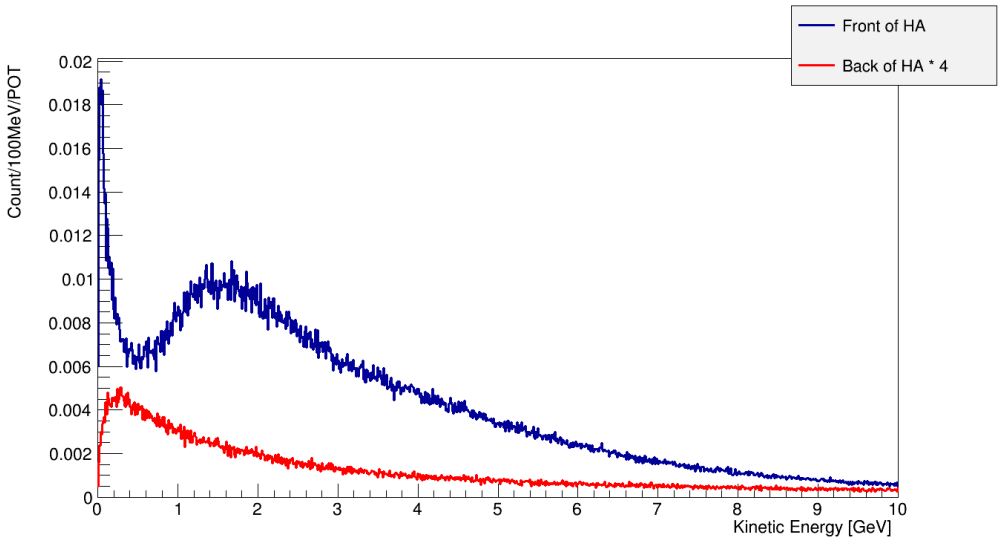

Figure 3.7: Muon energy distribution at front and back of absorber

geometry.

Looking into how specific neutrino detection rates change reveals that the ratio of near to far absorber-born counts does indeed change:

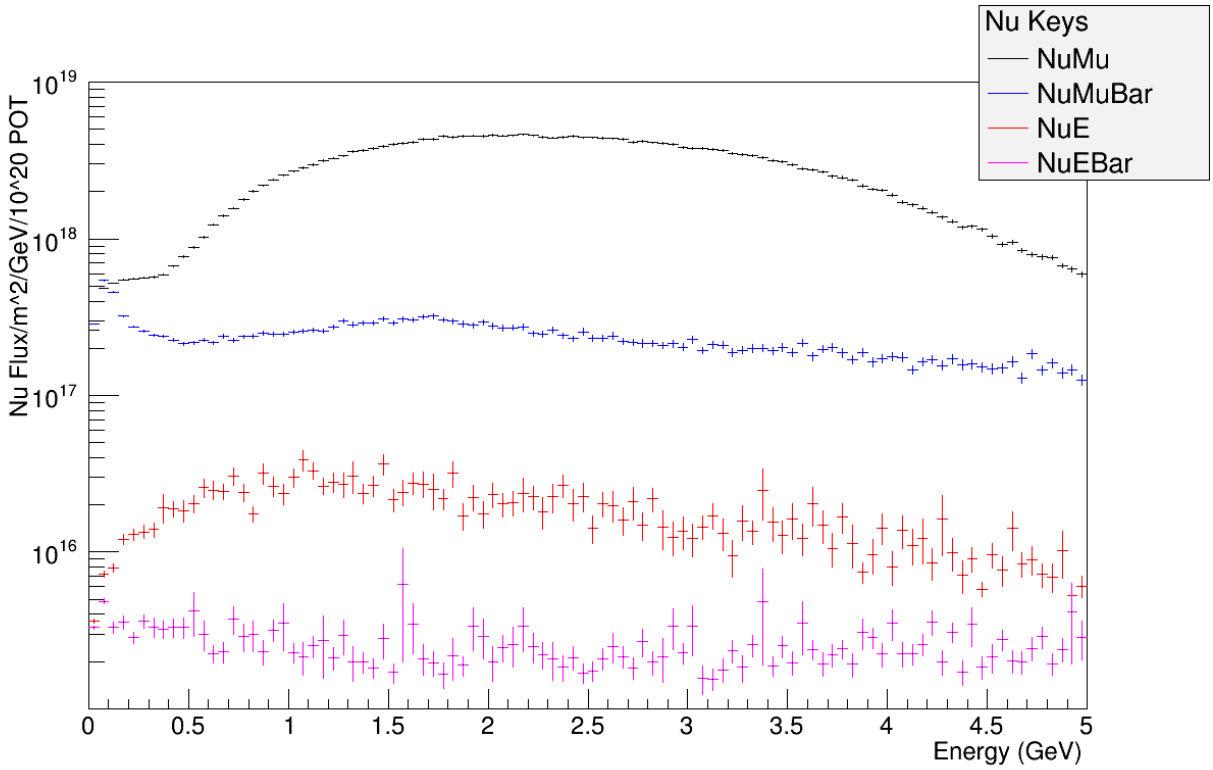

Figure 4.1: Neutrino flux of various flavors at the near detector.

Neutrino Mode	ν_μ	$\overline{\nu_\mu}$	ν_e	$\overline{\nu_e}$
Near	0.33%	3.32%	0.91%	2.61%
Far	0.13%	1.26%	0.41%	1.03%

Table 1: Percent of detector neutrino flux from absorber volumes

The percent contamination of absorber-born neutrinos at the near detector is more than double that of the far detector.

Plotting the neutrino flux at the far detector, we see a similar flux distribution.

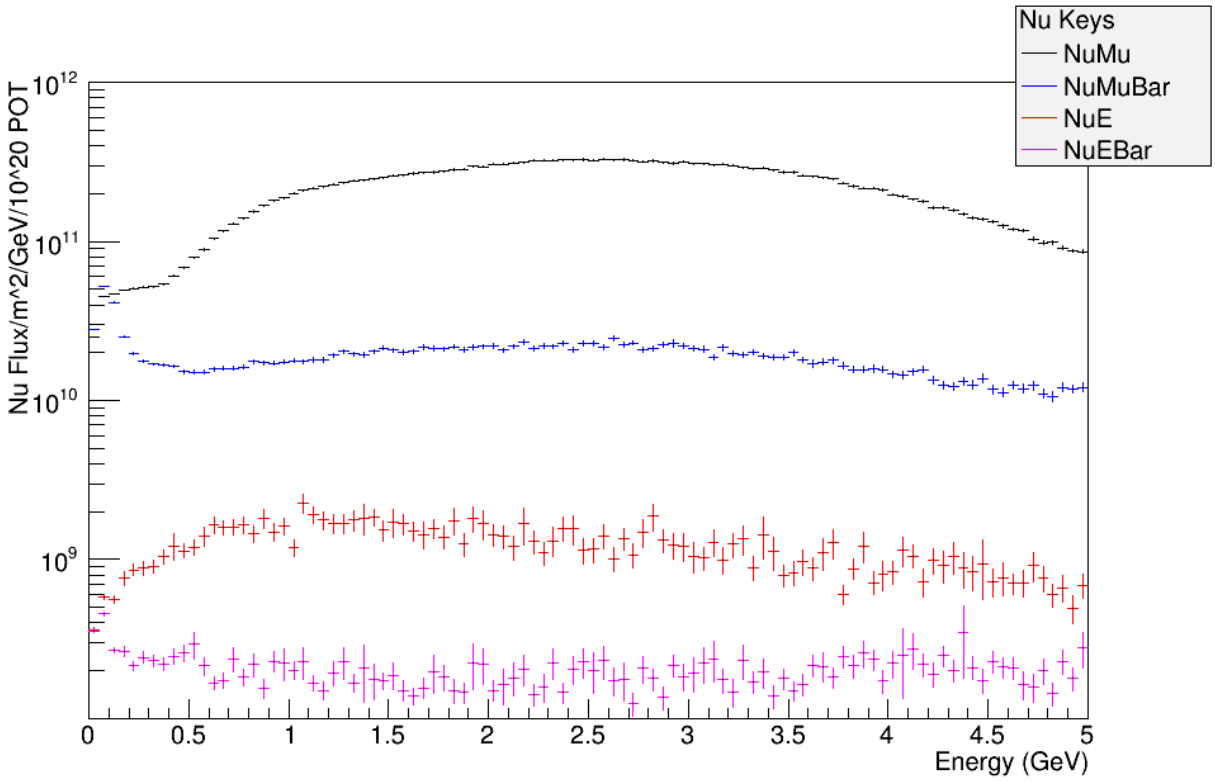

Figure 4.2: Neutrino flux of various flavors at the far detector.

The overall flux at the near Fig. 4.1 and far Fig. 4.2 detectors are useful, but of greater relevance to this study is the percent of flux of a given flavor from the absorber volumes, as a function of energy.

These plots Fig. 4.3 (found on last page) show how absorber-born neutrino count rates compare to the total neutrino count rate at the near and far detectors, as a function of energy. Here, then, are the most significant results of the study. At low energies (< 1 GeV) up to 10% of muon and anti-muon neutrinos detected come from absorber volumes (Fig. 4.3a and Fig. 4.3b).

4.1 Antineutrino mode

If we run our simulation with a negative current in the focusing horns, this is known as "antineutrino mode", as this will select the opposite sign particles for focusing, which will favor antineutrino production. The effects from the absorber are, as before:

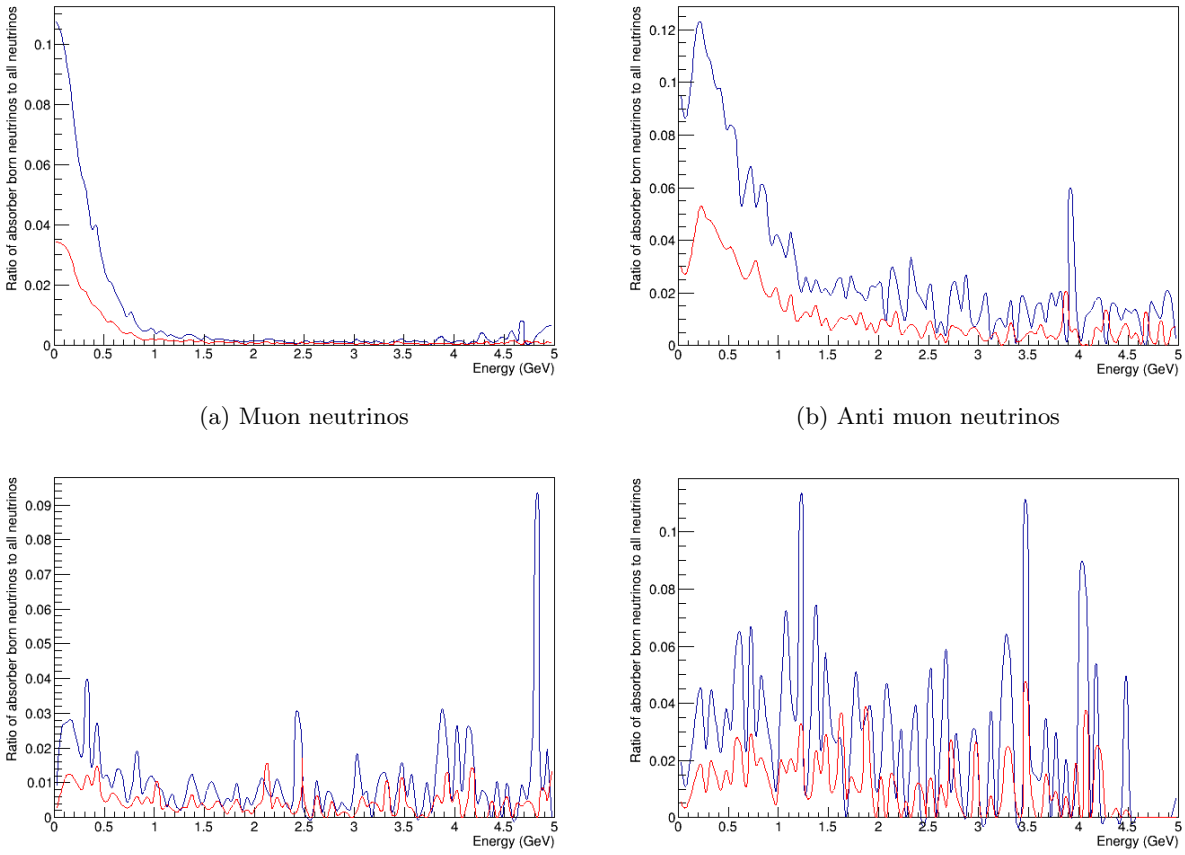

(a) Muon neutrinos

(b) Anti muon neutrinos

(c) Electron neutrinos

(d) Anti electron neutrinos

Figure 4.3: Ratio of absorber born to total neutrino flux at the detectors. Graphed by flavor. Far detector in red.

Antineutrino Mode	ν_μ	$\overline{\nu_\mu}$	ν_e	$\overline{\nu_e}$
Near	3.47%	0.31%	4.13%	0.60%
Far	1.29%	0.12%	1.68%	0.27%

Table 2: Percent of detector neutrino flux from absorber volumes (in antineutrino mode)

Comparing Table. 2 with Table. 1 we see the expected favoring of the opposite sign, though with an unexpected increase in ν_e production in the absorber.

5 Conclusions

Muon contamination from the hadron absorber is not a problem that can be swept under the rug. The neutrino contamination from the absorber volumes shown in Fig. 4.3 shows that contamination is a serious issue that needs a solution. Secondary muons from hadron absorber interactions have energy and momenta that are hard to predict, and are not insubstantial in contribution to total flux. The difference in total muon contamination and "important" muon contamination from absorber volumes (an order of magnitude) makes

the task of correlating muon counts with neutrino flux even more error-prone.

Not only is neutrino contamination an issue, it's an issue of varying magnitude at each detector, making correlation statistics more uncertain. The ratio plots of neutrino flux from the absorber regions to total flux as a function of energy Fig. 4.3 should shed some light on what would have been anomalous-seeming spikes. This absorber design, with low-density materials and internal voids, may result in significant contamination of muons used for monitoring and a significant change in the neutrino near/far flux ratio.

References

[1] LBNE-doc-10092

[2] LBNE-doc-10095

[3] LBNE-doc-11203

[4] https://sharepoint.fnal.gov/project/lbne/LBNE at Work/science doc pdfs/chapter_3_optim.pdf (figure 3.18)